

## MAGII-CAT V. ORIENTATION OF OUTFLOWS AND ACCRETION DETERMINE THE KINEMATICS AND COLUMN DENSITIES OF THE CIRCUMGALACTIC MEDIUM

NIKOLE M. NIELSEN<sup>1,2</sup>, CHRISTOPHER W. CHURCHILL<sup>2</sup>, GLENN G. KACPRZAK<sup>1</sup>, MICHAEL T. MURPHY<sup>1</sup>, AND JESSICA L. EVANS<sup>2</sup>

<sup>1</sup> Centre for Astrophysics and Supercomputing, Swinburne University of Technology, Hawthorn, Victoria 3122, Australia; nikolenielsen@swin.edu.au

<sup>2</sup> Department of Astronomy, New Mexico State University, Las Cruces, NM 88003, USA

Accepted to ApJ, September 12, 2015

### ABSTRACT

We investigate the dependence of gas kinematics and column densities in the MgII-absorbing circumgalactic medium on galaxy color, azimuthal angle, and inclination to trace baryon cycle processes. Our sample of 30 foreground isolated galaxies at  $0.3 < z_{\text{gal}} < 1.0$ , imaged with the *Hubble Space Telescope*, are probed by background quasars within a projected distance of  $20 < D < 110$  kpc. From the high-resolution ( $\Delta v \simeq 6.6$  km s<sup>-1</sup>) quasar spectra, we quantify the extent of the absorber velocity structure with pixel-velocity two-point correlation functions. Absorbers with the largest velocity dispersions are associated with blue, face-on ( $i < 57^\circ$ ) galaxies probed along the projected minor axis ( $\Phi \geq 45^\circ$ ), while those with the smallest velocity dispersions belong to red, face-on galaxies along the minor axis. The velocity structure is similar for edge-on ( $i \geq 57^\circ$ ) galaxies regardless of galaxy color or azimuthal angle, for red galaxies with azimuthal angle, and for blue and red galaxies probed along the projected major axis ( $\Phi < 45^\circ$ ). The cloud column densities for face-on galaxies and red galaxies are smaller than for edge-on galaxies and blue galaxies, respectively. These results are consistent with biconical outflows along the minor axis for star-forming galaxies and accreting and/or rotating gas, which is most easily observed in edge-on galaxies probed along the major axis. Gas entrained in outflows may be fragmented with large velocity dispersions, while gas accreting onto or rotating around galaxies may be more coherent due to large path lengths and smaller velocity dispersions. Quiescent galaxies may exhibit little-to-no outflows along the minor axis, while accretion/rotation may exist along the major axis.

*Keywords:* galaxies: evolution — galaxies: halos — quasars: absorption lines

### 1. INTRODUCTION

The circumgalactic medium (CGM) is generally defined as the bound gaseous halo surrounding galaxies which extends out to a few hundred kiloparsecs (e.g., Kacprzak et al. 2008; Steidel et al. 2010; Tumlinson et al. 2011; Rudie et al. 2012; Kacprzak et al. 2013; Nielsen et al. 2013a,b; Tumlinson et al. 2013; Werk et al. 2013). This region has increasingly been found to host some of the most important mechanisms involved in galaxy evolution through the baryon cycle, including gas accretion via the intergalactic medium and/or recycled accretion via the galactic fountain mechanism, galactic-scale outflowing winds, and merging satellite galaxies. The diffuse, multiphase nature of the CGM lends itself to study by way of absorption lines found in bright, background objects such as quasars or galaxies, or even in the spectrum of the host galaxy itself (i.e., the “down-the-barrel” approach).

Most work examining the low-ionization, cool ( $T \sim 10^4$  K) component of the CGM has been focused on MgII  $\lambda\lambda 2796, 2803$  doublet absorption in background quasar spectra as it is easily observed in the optical at redshifts  $0.1 < z < 2.5$  (e.g., Bergeron & Boissé 1991; Steidel et al. 1994; Guillemin & Bergeron 1997; Steidel et al. 1997; Churchill et al. 2005; Barton & Cooke 2009; Kacprzak et al. 2011; Lan et al. 2014), and for a range of HI column densities ( $16 \leq \log N(\text{HI}) \leq 22$ , e.g., Bergeron & Stasińska 1986; Steidel & Sargent 1992; Churchill et al. 2000; Rao & Turnshek 2000; Rigby et al. 2002). The MgII ion is well-known to be a tracer of the steps involved in the baryon cycle including accretion, rotating material merging onto the galaxy, and outflows. MgII absorbing gas may also be associated with merging satellites which are in the process of being tidally stripped and/or have ongoing star formation driven outflows.

Accreting gas in the form of filaments from the cosmic web and/or recycled accretion from past outflows has been found to lie near the plane of the galaxy disk both in observations (e.g., Steidel et al. 2002; Kacprzak et al. 2010; Martin et al. 2012; Rubin et al. 2012; Bouché et al. 2013) and in simulations (e.g., Stewart et al. 2011; Ford et al. 2014). Simulations have also shown that this material forms an extended (out to  $\sim 0.3R_{\text{vir}}$ ), warped disk that co-rotates with the galaxy when viewed in edge-on orientations (e.g., Stewart et al. 2011; Danovich et al. 2012, 2015). Direct observations of infalling material have been few due to the small covering fraction of the accreting material (at least 6%; e.g., Martin et al. 2012; Rubin et al. 2012) and because outflows dominate the absorption profile, though the spectra used in these works have low resolution with  $\Delta v > 150$  km s<sup>-1</sup>, which may contribute to the low detection rate. Nonetheless, accretion and rotation signatures may include velocities that are bound to the host galaxy, but are greater than or comparable to projected rotational velocities of the disk for edge-on galaxies probed along the projected major axis. The velocities of these absorbers likely lie to one side of the galaxy’s systemic velocity (Steidel et al. 2002; Kacprzak et al. 2010; Stewart et al. 2011; Bouché et al. 2013), especially when viewing galaxies in nearly edge-on inclinations.

Based on low-resolution ( $\Delta v > 150$  km s<sup>-1</sup>) spectra, outflows from galactic-scale winds due to star formation and/or supernovae feedback are often invoked to explain the presence of MgII absorption (e.g., Rubin et al. 2010; Bouché et al. 2012; Martin et al. 2012; Bordoloi et al. 2014a,b; Rubin et al. 2014; Kacprzak et al. 2014). A down-the-barrel approach was used in Weiner et al. (2009) and Rubin et al. (2010), and these authors show that, in stacked galaxy spec-

tra, outflows are commonly observed in face-on orientations due to the observed blueshift of material being pushed out of the host galaxy in the direction of the observer. Using both a down-the-barrel sightline and a transverse sightline through a single galaxy, Kacprzak et al. (2014) find that the sightlines are kinematically coupled and associated with outflowing material despite the large projected distance (58 kpc) between the two. In this case, the transverse quasar sightline is aligned with the galaxy projected minor axis. Finally, by modeling galactic winds to reproduce the absorption found in seven transverse sightlines, most of which are aligned with the galaxy projected minor axis, Bouché et al. (2012) were able to estimate properties of the winds such as wind speeds. All of this work is consistent with the picture of biconical, polar outflows whose signatures include broad, complex absorption profiles spanning hundreds of  $\text{km s}^{-1}$  that cannot be explained by rotation (Veilleux et al. 2005). Such a biconical outflow model is also applicable to our own Milky Way Galaxy (Fox et al. 2015).

Merging satellite galaxies may also be a source of Mg II absorption in the CGM. For  $z > 0.3$  the low luminosities of satellite galaxies makes it difficult to directly observe such satellites. In fact, Martin et al. (2012) found a redshifted absorber with respect to the targeted galaxy and associated it with a satellite that was clearly detected in their galaxy images, but this was the only case out of their sample of over 200 galaxies, indicating that satellites as the source of absorption is likely rare ( $< 1\%$  probability). Examining the azimuthal angle dependence of satellites around host galaxies, Yang et al. (2006) found that satellites within  $D = 700$  kpc tend to be isotropically distributed around blue galaxies, but are preferentially located along the major axis of red galaxies. This result has been found with a variety of data sets, which are summarized in Yang et al. (2006), as well as in simulations (most recently by Dong et al. 2014).

Detailed absorber kinematics for a large absorber–galaxy sample, which are required to provide insight into the motions of the gas involved in the baryon cycle and constrain simulations, have thus far remained elusive due to the need to stack low-resolution spectra. Even without needing to stack the spectra, much of the velocity structure is washed out by the low resolution. Most of the previous work examining Mg II absorbers associated with baryon cycle processes have reported that the Mg II equivalent width depends strongly on inclination and/or azimuthal angle (e.g., Bordoloi et al. 2011; Kacprzak et al. 2011; Bouché et al. 2012; Kacprzak et al. 2012; Bordoloi et al. 2014a,b), however equivalent width does not provide a detailed picture of the gas kinematics. This is especially true since equivalent width depends on the velocity spread of absorption and the column densities, which in turn depend on the line-of-sight geometry, metallicity, and ionization conditions of the absorbers. We therefore make use of a subsample of galaxies in the Mg II Absorber–Galaxy Catalog (MAGIIICAT; Nielsen et al. 2013a,b; Churchill et al. 2013) for which we have high-resolution ( $R \sim 45,000$ ,  $\Delta v \simeq 6.6 \text{ km s}^{-1}$ ) background quasar spectra, in addition to the colors and orientations of the galaxies themselves. With these line-of-sight data, we can study the detailed kinematics of Mg II absorbers and examine if the enhanced detection rates and larger equivalent widths for particular orientations are due to velocity spreads, column densities, or some combination of both.

In a previous work, Kacprzak et al. (2012) examined the

equivalent widths of Mg II absorbers with galaxy orientation for a subset of absorber–galaxy pairs from MAGIIICAT (Nielsen et al. 2013a,b) by modeling the galaxies and measuring the azimuthal angles at which background quasars probe the CGM. They found that Mg II absorption prefers to be located along the major and minor axes of blue galaxies, while there is no such preference for absorbers located around red galaxies (a result confirmed with a larger, statistical sample by Lan et al. 2014), or for sightlines in which no absorption is detected (nonabsorbers) regardless of galaxy color. Kacprzak et al. (2012) also found a tendency for Mg II equivalent widths to be larger along the minor axis than the major axis, possibly an indication of probing more enriched outflowing material along the minor axis.

In this paper, we expand upon our previous work and examine the kinematics of absorbing gas as a function of galaxy color and inclination as well as the azimuthal angle at which the galaxy is probed by using Mg II absorber pixel-velocity two-point correlation functions (TPCFs, described in detail by Nielsen et al. 2015) and cloud column densities. This paper is organized as follows. Section 2 describes the sample, our methods for analyzing the spectra and data, and how we calculate the TPCFs. Section 3 details how the absorber kinematics (TPCFs) and cloud column densities differ for galaxies of various colors, azimuthal angles, and inclinations. In Section 4 we place our kinematics results in the context of the baryon cycle and discuss the implications. Finally, we summarize and conclude our findings in Section 5. We adopt a  $\Lambda$ CDM cosmology ( $H_0 = 70 \text{ km s}^{-1} \text{ Mpc}^{-1}$ ,  $\Omega_M = 0.3$ ,  $\Omega_\Lambda = 0.7$ ) throughout this paper.

## 2. SAMPLE AND DATA ANALYSIS

### 2.1. Data

We use a sample of 30 spectroscopically confirmed ( $0.3 < z_{\text{gal}} < 1.0$ ) Mg II absorption-selected galaxies from the Mg II Absorber–Galaxy Catalog (MAGIIICAT; Nielsen et al. 2013a,b). The galaxies are isolated to the limits of the data, where isolation is defined as having no spectroscopically identified neighbor within a projected distance of 100 kpc or a line-of-sight velocity of  $500 \text{ km s}^{-1}$ . Each galaxy has been imaged with WFPC2/HST in the F702W band and we have a rest-frame  $B-K$  color for each galaxy which was determined as described in Nielsen et al. (2013b).

All galaxies were modeled using GIM2D (Simard et al. 2002) to obtain quantified morphological parameters, inclinations, and position angles. Full details of the method used and the morphological properties of most galaxies in our sample are presented in Kacprzak et al. (2011). We define inclinations of  $i = 0^\circ$  as face-on and  $i = 90^\circ$  as edge-on. We convert position angles to an “azimuthal angle” which describes where a background quasar sightline is located with respect to the projected major axis of the galaxy. An azimuthal angle of  $\Phi = 0^\circ$  is defined as having the quasar line of sight along the projected galaxy major axis and  $\Phi = 90^\circ$  as having the sightline along the projected minor axis. Figure 1 illustrates our galaxy orientation definitions with azimuthal angle in panel (a) and inclination in panel (b).

The CGM of each galaxy is probed by a nearby (projected on the sky distance of  $20 < D < 110$  kpc) background quasar for which we have a high-resolution HIRES/Keck or UVES/VLT spectrum. We refer the reader to Churchill (1997), Churchill & Vogt (2001), Churchill et al. (2003), Evans (2011), and Kacprzak et al. (2011) for the spectra, full

**Table 1**  
TPCF Velocity Measurements

Galaxy Sample	# Gals	Cut	Cut	$\Delta v(50)^a$	$\Delta v(90)^a$
Figure 2					
Face-on	17	$i < 57^\circ$	...	$69^{+8}_{-9}$	$200^{+15}_{-21}$
Edge-on	13	$i \geq 57^\circ$	...	$64^{+4}_{-6}$	$149^{+10}_{-14}$
Major Axis	15	$\Phi < 45^\circ$	...	$55^{+7}_{-13}$	$146^{+13}_{-32}$
Minor Axis	15	$\Phi \geq 45^\circ$	...	$73^{+5}_{-7}$	$192^{+15}_{-21}$
Face-on – Major Axis	10	$i < 57^\circ$	$\Phi < 45^\circ$	$45^{+6}_{-6}$	$124^{+20}_{-22}$
Face-on – Minor Axis	7	$i < 57^\circ$	$\Phi \geq 45^\circ$	$84^{+8}_{-13}$	$220^{+13}_{-25}$
Edge-on – Major Axis	5	$i \geq 57^\circ$	$\Phi < 45^\circ$	$73^{+10}_{-20}$	$171^{+23}_{-45}$
Edge-on – Minor Axis	8	$i \geq 57^\circ$	$\Phi \geq 45^\circ$	$60^{+4}_{-5}$	$141^{+8}_{-11}$
Figure 3					
Blue – Major Axis	5	$B-K < 1.4$	$\Phi < 45^\circ$	$61^{+9}_{-11}$	$162^{+20}_{-23}$
Blue – Minor Axis	10	$B-K < 1.4$	$\Phi \geq 45^\circ$	$81^{+8}_{-9}$	$209^{+16}_{-23}$
Red – Major Axis	10	$B-K \geq 1.4$	$\Phi < 45^\circ$	$51^{+10}_{-13}$	$135^{+20}_{-36}$
Red – Minor Axis	5	$B-K \geq 1.4$	$\Phi \geq 45^\circ$	$52^{+1}_{-4}$	$123^{+2}_{-9}$
Figure 4					
Blue – Face-on	8	$B-K < 1.4$	$i < 57^\circ$	$88^{+8}_{-10}$	$227^{+12}_{-19}$
Blue – Edge-on	7	$B-K < 1.4$	$i \geq 57^\circ$	$61^{+4}_{-8}$	$143^{+9}_{-19}$
Red – Face-on	9	$B-K \geq 1.4$	$i < 57^\circ$	$40^{+3}_{-4}$	$97^{+6}_{-9}$
Red – Edge-on	6	$B-K \geq 1.4$	$i \geq 57^\circ$	$62^{+7}_{-14}$	$147^{+15}_{-33}$

<sup>a</sup> km s<sup>-1</sup>

details of the reduction and analysis, and the detection and Voigt profile (VP) fitting of Mg II  $\lambda\lambda 2796, 2803$  absorption. We measure Mg II equivalent widths and, from the VP fitting, we obtain VP component (cloud) column densities, velocities, and Doppler  $b$  parameters. Velocity zero points are defined as the median velocity of the apparent optical depth distribution of Mg II absorption (Churchill 1997).

For our TPCF analysis, we use only the velocities of pixels that reside in regions where absorption is formally detected. These regions are defined as “kinematic subsystems” in Churchill & Vogt (2001) and their velocity bounds are determined by searching the spectra to either side of the subsystem centroids for the point at which the significance in the per pixel equivalent width falls below  $1\sigma$ . We enforce a sensitivity cut to these regions of  $W_r(2796) \geq 0.04 \text{ \AA}$  to account for differences in the quality of our spectra (Nielsen et al. 2015). We are  $\sim 95\%$  complete to this detection sensitivity within  $\pm 800 \text{ km s}^{-1}$  for all absorbers in our sample. This sensitivity cut is used to ensure that we can detect absorption uniformly throughout our sample. Thus, the results in this paper apply to Mg II absorption with  $W_r(2796) \geq 0.04 \text{ \AA}$ , and therefore samples only those regions of the CGM for which the temperature, metallicity, ionization, and line-of-sight conditions give rise to gas detected with Mg II for our sample.

We slice the sample into several subsamples based on galaxy rest-frame  $B-K$  color, azimuthal angle,  $\Phi$ , and inclination,  $i$ . Galaxy color and azimuthal angle cuts were determined by calculating the median values for the sample

we present here (similar to the method used in Nielsen et al. 2013a,b). Our inclination cut was defined by the average inclination of galaxies in the universe,  $i = 57.3^\circ$  (for a derivation, see the appendix of Law et al. 2009). We tabulate the characteristics of each subsample in Table 1 including the subsample names, number of galaxies in each subsample, and the median value(s) by which the sample was cut. The  $B-K$  color cut we use to separate our sample into “blue” and “red” galaxies is strictly to indicate whether the galaxy is more likely to be star-forming (blue) or passive (red), rather than indicating morphological types such as early-type or late-type galaxies. Figure 1 illustrates our subsample cuts for azimuthal angle (panel (a)) and inclination (panel (b)).

We caution that, in our sample, a weak trend exists between  $B-K$  and halo mass,  $\log(M_h/M_\odot)$ , (Kendall  $\tau$  rank correlation test,  $2.1\sigma$ ) where redder galaxies tend to be more massive. We find that, with the exception of eight galaxies, blue galaxies tend to be low mass while red galaxies tend to be high mass (see Nielsen et al. 2015, for details). Therefore, the color dependencies in our results are more accurately color-mass dependencies.

To rule out the possibility that any differences in our results are due to biased distributions in azimuthal angle and inclination, we ran a one-dimensional Kolmogorov–Smirnov (KS) test for both orientation measures. We find that the azimuthal angles and inclinations of galaxies in our sample are consistent with unbiased samples at the  $0.6\sigma$  and  $2.3\sigma$  levels, respectively. Additionally, rank-correlation tests between  $\Phi$  or  $i$

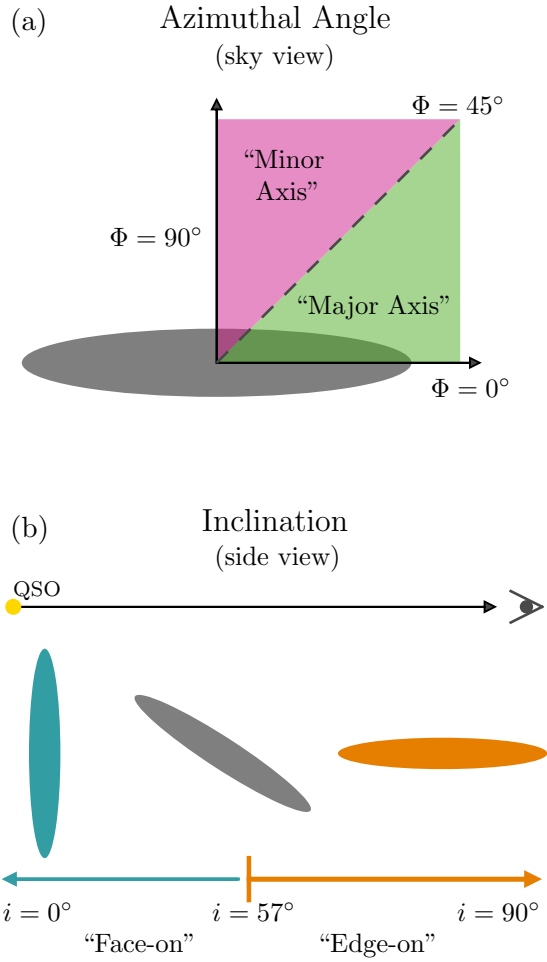


**Figure 1.** Diagram demonstrating galaxy azimuthal angle and inclination subsamples. Panel (a) presents an on-the-sky view of the azimuthal angle around an inclined galaxy (gray ellipse). An azimuthal angle of  $\Phi = 0^\circ$  is defined as the projected galaxy major axis, while  $\Phi = 90^\circ$  is the projected galaxy minor axis. Galaxies which are probed by quasar sightlines at  $0^\circ \leq \Phi < 45^\circ$  are included in the “major axis” subsample (green shaded region), while those probed at  $45^\circ \leq \Phi \leq 90^\circ$  are included in the “minor axis” subsample (pink shaded region). Colors in this panel correspond to the colors in Figures 2, 3, and 6. Panel (b) presents a side view of three galaxies with different inclinations whose CGM is probed by a background quasar. We define “face-on” galaxies as those with  $0^\circ \leq i < 57^\circ$  (blue ellipse and arrow) while “edge-on” galaxies are those with  $57^\circ \leq i \leq 90^\circ$  (orange ellipse and arrow, including the gray ellipse). An inclination of  $i = 57^\circ$  is the value for which we cut our sample and corresponds to the minimum inclination for an “edge-on” galaxy (gray ellipse). Colors and arrow line widths in this panel correspond to the colors in Figures 2, 4, and 5.

and galaxy properties such as rest-frame  $B-K$  color show no correlations. Therefore, any differences we see in our results are likely not due to underlying sample biases.

## 2.2. Pixel-Velocity Two-Point Correlation Functions

Throughout this paper we examine absorber pixel-velocity two-point correlation functions (TPCFs), which are a measure of the *internal* absorber velocity dispersion. We remind the reader that the absorber–galaxy sample presented here is an absorption-selected sample with an equivalent width detection threshold of  $W_r(2796) \geq 0.4 \text{ \AA}$  (see Section 2.1).

To construct the TPCF, we first define a subsample of galaxies, e.g., blue galaxies, and examine the associated absorbers. We obtain the velocities of all pixels that reside

only in spectral regions where Mg II  $\lambda 2796$  absorption is formally detected using the detection methods of Churchill & Vogt (2001), who refer to these regions as “kinematic subsystems.” After pooling all of the absorbing pixels from every line-of-sight in the galaxy subsample together, we then calculate the velocity differences of each possible pair of pixels and take their absolute value to get  $\Delta v_{\text{pixel}}$ . We bin up these pixel-velocity separations and normalize each bin by the total number of pixel pairs in the subsample for comparison between different galaxy subsamples. Thus, the TPCF is a probability distribution function. We use a bin size of  $10 \text{ km s}^{-1}$ , which corresponds to roughly one resolution element of both the HIRES/Keck and UVES/VLT spectrographs (three pixels per resolution element, with a resolution of  $\sim 6.6 \text{ km s}^{-1}$ ).

To obtain the uncertainties on the TPCF, we conduct a bootstrap analysis for 100 realizations, where the maximum number of realizations allowed for a sample size of five (our smallest sample) with replacement is 126. More realizations than this begin repeating permutations too often. We calculate  $1\sigma$  standard deviations from the mean of the bootstrap realizations in each bin.

We quantitatively characterize the TPCFs by measuring the velocity separations within which 50% and 90% of the area under the TPCF distribution is located,  $\Delta v(50)$  and  $\Delta v(90)$ , respectively. Uncertainties on these values are obtained from the bootstrap analysis and represent  $1\sigma$  deviations from the mean of the bootstrap realizations. The values for  $\Delta v(50)$  and  $\Delta v(90)$  are tabulated in Table 1 for each subsample.

## 3. RESULTS

### 3.1. TPCFs: Galaxy Inclinations and Azimuthal Angles

In Figure 2 we present TPCFs for galaxy subsamples cut by galaxy azimuthal angle,  $\Phi$ , and/or inclination,  $i$ , for all galaxy colors,  $B-K$ . Solid lines represent the TPCF for each subsample while shaded regions indicate the  $1\sigma$  uncertainties on the TPCFs from the bootstrap analysis described in Section 2.2. Colors for azimuthal angle and inclination subsamples correspond to those in Figure 1(a) and (b), respectively. In the top row we compare face-on and edge-on galaxy subsamples at all azimuthal angles (panel (a)), along the projected minor axis (panel (b)), and along the projected major axis (panel (c)). In the bottom row, we compare galaxies probed along the major and minor axes for galaxies at all inclinations (panel (d)), edge-on galaxy subsamples (panel (e)), and face-on galaxy subsamples (panel (f)). In each panel we present the results of a chi-squared test comparing the binned data (TPCFs) for each plotted subsample pair, including the significance, reduced chi-squared value,  $\chi^2_\nu$ , and degrees of freedom,  $\nu$ .

In Figure 2(a) we examine bivariate trends in the absorber TPCFs for galaxies with “face-on” ( $i < 57^\circ$ ) and “edge-on” ( $i \geq 57^\circ$ ) inclinations for all colors and probed at all azimuthal angles. Absorbers in face-on galaxies have larger velocity dispersions than those in edge-on galaxies. A chi-squared test yields the result that the null hypothesis that the TPCFs are drawn from the same population can be ruled out at the  $8.7\sigma$  level. While the chi-squared test result is significant, we find that the  $\Delta v(50)$  measurements are consistent within uncertainties for face-on and edge-on galaxies but the value of  $\Delta v(90)$  is larger for face-on galaxies. Therefore, the difference between these two distributions is due to the large velocity dispersion tail in face-on galaxies.

We also examine absorption associated with galaxies probed along the “major axis” ( $\Phi < 45^\circ$ ) and “minor axis”

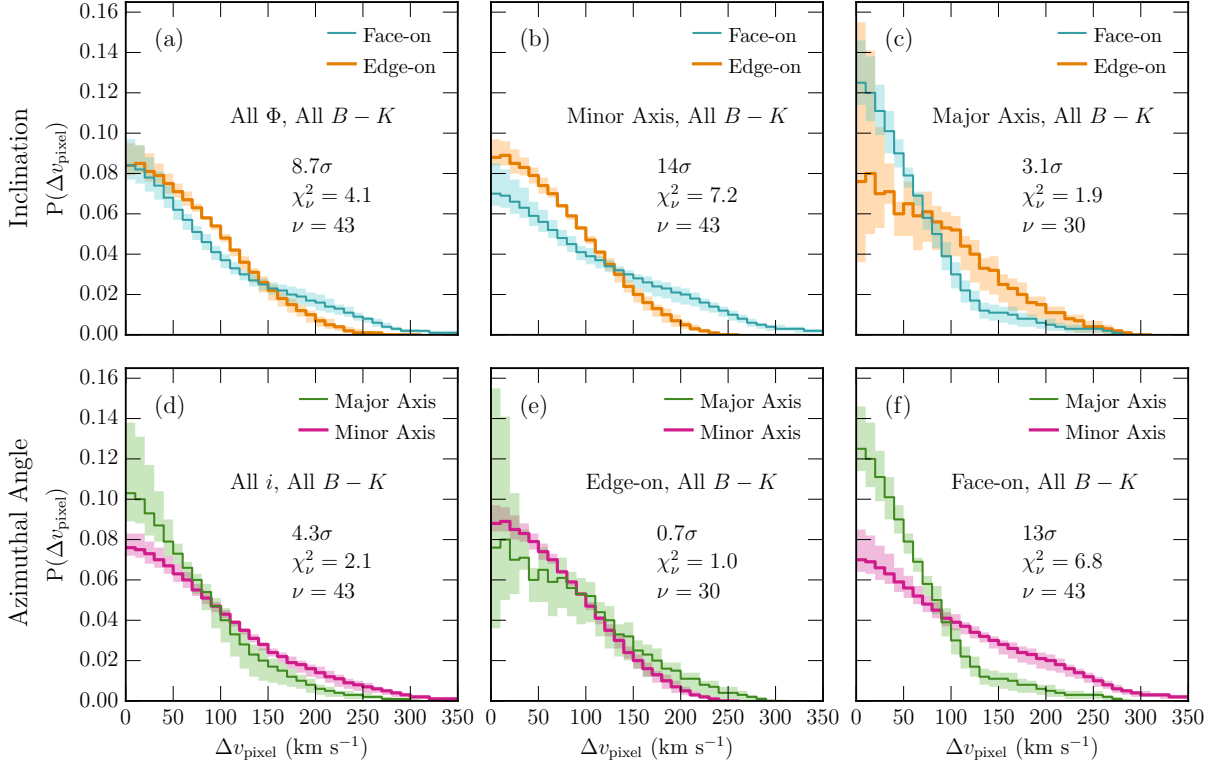


**Figure 2.** Pixel-velocity two-point correlation functions examining how the spread in the pixel velocities of absorbers differs when probing galaxies of different inclinations and azimuthal angles (for all galaxy colors,  $B-K$ ). Panels (a), (b), and (c) compare TPCFs of face-on ( $i < 57^\circ$ ) and edge-on ( $i \geq 57^\circ$ ) galaxies for all  $\Phi$ ,  $\Phi \geq 45^\circ$ , and  $\Phi < 45^\circ$ , respectively. Panels (d), (e), and (f) examine how the TPCFs along the major axis ( $\Phi < 45^\circ$ ) and minor axis ( $\Phi \geq 45^\circ$ ) differ for all  $i$ ,  $i \geq 57^\circ$ , and  $i < 57^\circ$ , respectively. In each panel the TPCF is represented as a solid line while shaded regions are the  $1\sigma$  bootstrap uncertainties. We list the significance of a chi-squared test comparing the TPCFs in each panel in addition to the reduced chi-squared value,  $\chi^2_\nu$ , and the degrees of freedom,  $\nu$ . We see a broader velocity dispersion for face-on galaxies than for edge-on galaxies when all azimuthal angles are considered (panel (a)). We also see a larger velocity dispersion for galaxies probed along the minor axis than along the major axis when all inclinations are considered (panel (d)). This latter result becomes highly significant for face-on galaxies where the minor axis dispersion is greater than that for the major axis (panel (f)). Conversely, there is no difference in the velocity dispersion with azimuthal angle for edge-on orientations (panel (e)). Thus, the velocity dispersion is greatest for face-on galaxies probed along the projected minor axis.

( $\Phi \geq 45^\circ$ ) in Figure 2(d) for all inclinations and colors and find that absorbers located in galaxies probed along the minor axis have larger velocity dispersions than those along the major axis ( $4.3\sigma$ ). Both  $\Delta v(50)$  and  $\Delta v(90)$  are larger for the minor axis sample than the major axis. For this TPCF pair and the rest in this paper, the measurements of both  $\Delta v(50)$  and  $\Delta v(90)$  reflect the chi-squared test results, i.e., where we find an insignificant chi-squared value when comparing galaxy subsamples, we also find values of  $\Delta v(50)$  and  $\Delta v(90)$  that are consistent within uncertainties between subsamples.

While we find significant differences in the absorber TPCFs with inclination or azimuthal angle, both orientation measures are important for describing the precise location of an absorber around a galaxy. Therefore, in Figure 2 we present a multivariate analysis comparing the absorber TPCFs for face-on and edge-on galaxies probed along the minor axis (panel (b)) and the major axis (panel (c)). In both panels we find that the velocity structure for absorbers probed in face-on galaxies is significantly different from those in edge-on galaxies. Along the minor (major) axis, the velocity dispersion of absorbers is greater (smaller) for face-on galaxies than edge-on galaxies with a significance of  $14\sigma$  ( $3.1\sigma$ ) in panel (b) (panel (c)).

We also compare absorber TPCFs for galaxies probed along the major and minor axes for edge-on galaxies (panel (e)) and face-on galaxies (panel (f)). We find that absorbers located in

edge-on galaxies have similar velocity dispersions regardless of the azimuthal angle at which the galaxy is probed (panel (e),  $0.7\sigma$ ). On the other hand, we find a highly significant difference ( $13\sigma$ ) for face-on galaxies probed along the major and minor axes in Figure 2(f) where the absorber velocity dispersions are much greater along the minor axis than the major axis. In fact, both  $\Delta v(50)$  and  $\Delta v(90)$  for the face-on, minor axis subsample are roughly twice as large as the face-on, major axis subsample.

### 3.2. TPCFs: Galaxy Colors and Orientations

We also study the differences in absorber TPCFs for galaxies of various orientations and galaxy color. In Figure 3, we present subsamples cut by azimuthal angle,  $\Phi$ , and galaxy rest-frame color,  $B-K$ , for all galaxy inclinations. We find no significant difference ( $0.2\sigma$ ) in absorber velocity dispersions along the major axis in “blue” ( $B-K < 1.4$ ) and “red” ( $B-K \geq 1.4$ ) galaxies (panel (a)) or for absorbers hosted by red galaxies along the major and minor axes (panel (d)). The only TPCF that is significantly different from the rest of the subsamples is the blue, minor axis subsample. This blue, minor axis subsample has a significantly larger absorber velocity dispersion than either the red, minor axis subsample (panel (b),  $16\sigma$ ) or the blue, major axis subsample (panel (c),  $3.6\sigma$ ). While  $\Delta v(50)$  and  $\Delta v(90)$  are nearly identical for the red, major axis subsample, the red, minor axis subsample, and the

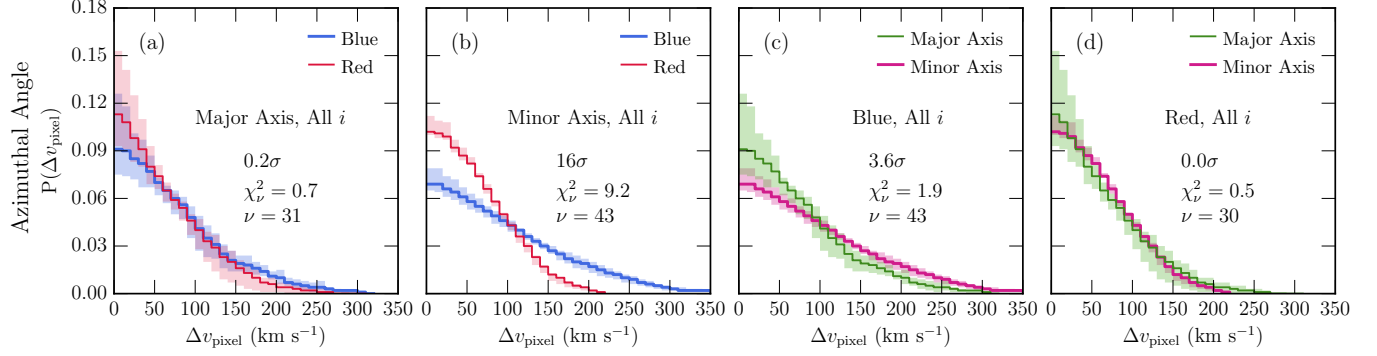


**Figure 3.** Pixel-velocity two-point correlation functions for subsamples cut by galaxy rest-frame  $B-K$  color and azimuthal angle. Lines, shading, and the results of a chi-squared test comparing subsamples are plotted as in Figure 2. For all inclinations, blue and red galaxy TPCFs are compared along the major axis ( $\Phi < 45^\circ$ ) and minor axis ( $\Phi \geq 45^\circ$ ) in panels (a) and (b), respectively. Panels (c) and (d) present the TPCFs of blue and red galaxies, respectively, at different azimuthal angles. The velocity dispersions are all statistically consistent (panels (a) and (d)) with the exception of large dispersions for the blue, minor axis subsample.

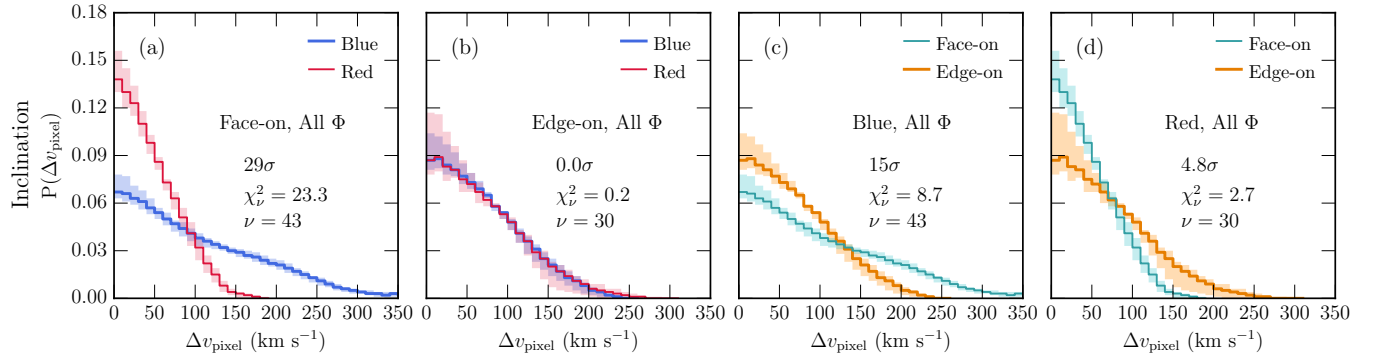


**Figure 4.** Pixel-velocity two-point correlation functions for subsamples cut by galaxy rest-frame  $B-K$  color and inclination. Lines, shading, and the results of a chi-squared test comparing subsamples are plotted as in Figure 2. For all azimuthal angles, we compare the TPCFs of blue and red face-on ( $i < 57^\circ$ ) galaxies in panel (a) and edge-on ( $i \geq 57^\circ$ ) galaxies in panel (b). Panels (c) and (d) compare the TPCFs of blue and red galaxies, respectively, at different inclinations. We find dramatic differences between the absorber velocity dispersions for blue and red galaxies for face-on orientations (panel (a)) where blue galaxies have much larger velocity dispersions than red galaxies, but we find no differences between blue and red for edge-on orientations (panel (b)).

blue, major axis subsample, the measurements for the blue, minor axis subsample are larger than the rest.

In Figure 4, we examine absorber TPCFs of subsamples sliced by inclination,  $i$ , and  $B-K$  color. Absorbers located around edge-on galaxies have similar velocity dispersions (for all  $\Phi$ ) regardless of galaxy color ( $0\sigma$ , Figure 4(b)). The values of  $\Delta v(50)$  and  $\Delta v(90)$  for edge-on blue and red subsamples are nearly identical and consistent within uncertainties. On the other hand, absorbers around face-on galaxies at all azimuthal angles in Figure 4(a) are dramatically different for blue and red galaxies. The absorber velocity dispersions are much greater ( $29\sigma$ ) for face-on, blue galaxies than for face-on, red galaxies, which are more highly peaked at low velocity separations. The  $\Delta v(50)$  and  $\Delta v(90)$  measurements are roughly twice as large for the face-on, blue subsample than the face-on, red subsample. The velocity dispersions of absorbers hosted by both blue and red galaxies in Figures 4(c) and 4(d) depend on the observed inclination, but differ in their trends; blue (red) galaxies have larger velocity dispersions for face-on (edge-on) inclinations than for edge-on (face-on) inclinations. This is due to the significant differences in face-on inclinations (Figure 4(a)) between blue and red galaxies (larger velocity dispersions for blue galaxies than red galaxies) and the nearly identical TPCFs for edge-on blue and red galaxies in panel (b).

### 3.3. Cloud Column Densities and Velocities

To obtain further understanding of the CGM material being probed for each orientation presented in the TPCFs, we plot cloud (VP component) column densities and velocities in Figure 5. Clouds plotted in panel (a) are associated with galaxies probed along the minor axis. In panel (b), clouds are associated with galaxies probed along the major axis. Scatter plots show the cloud column densities and velocities from Voigt profile fitting, where vertical dashed lines on the scatter plots at  $\pm 100 \text{ km s}^{-1}$  are to help guide the eye between panels. Points are colored by galaxy color,  $B-K$ , while point types represent galaxy inclination,  $i$ . Histograms to the left and right in each panel present the distribution of cloud column densities for galaxies sliced by (left) galaxy color and (right) inclination, where the indicated significance is the result of a KS test between subsamples for the unbinned data. Finally, the histograms on top and bottom show the distribution of pixel velocities (rather than cloud velocities) used to calculate the TPCFs for subsamples cut by galaxy color (bottom) and inclination (top). The result of an F-test<sup>1</sup> between the unbinned pixel velocities of each subsample pair is indicated next to the top and bottom histograms. In each case, the pixel velocity F-test results show similar results as the TPCF chi-squared test,

<sup>1</sup> The F-test is designed to measure whether two sample distributions have similar or different dispersions; it is sensitive to the tails of the distributions.

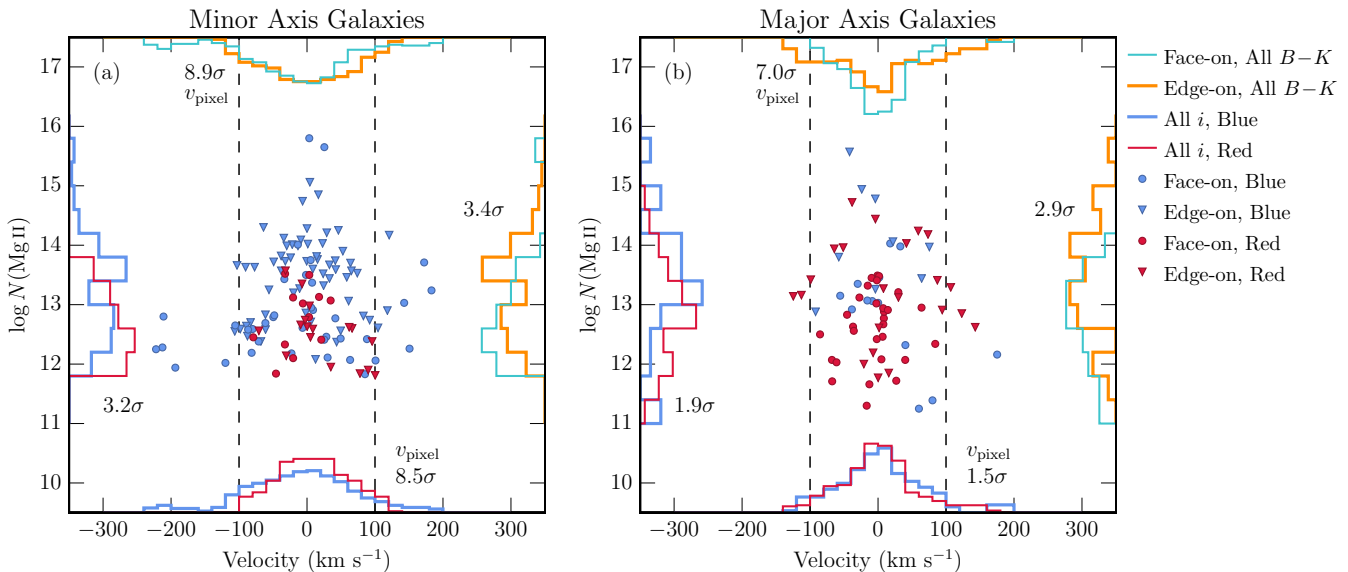


**Figure 5.** Cloud (VP component) column densities and velocities, and pixel velocities for galaxy subsamples sliced by inclination and galaxy color for galaxies probed along (a) the minor axis ( $\Phi \geq 45^\circ$ ) and (b) the major axis ( $\Phi < 45^\circ$ ). Scatter plots show the modeled cloud velocities and column densities. Blue points represent blue galaxies, red points are red galaxies, circles are face-on galaxies, and diamonds are edge-on galaxies. Vertical dashed lines at  $\pm 100 \text{ km s}^{-1}$  are provided to help guide the reader’s eye between panels. Histograms on the left and right of each panel show the distribution of cloud column densities for subsamples sliced by (left) galaxy color,  $B-K$ , and (right) inclination,  $i$ . The quoted significance near the column density histograms is the result of a KS test between plotted subsamples. Top and bottom histograms of each panel present the distribution of pixel (not cloud) velocities for subsamples cut by (bottom) galaxy color and (top) inclination. The significances quoted for the top and bottom histograms are for an F-test comparing the variance in the distribution of pixel velocities for each pair of plotted subsamples. All histograms are normalized by the total number of data points in each subsample. In general, we find that clouds with larger velocities relative to the optical depth median velocity have smaller column densities, while those with larger column densities have smaller velocities relative to the optical depth median velocity. We find that the cloud column density distributions are statistically consistent for galaxies probed along the major axis (panel (b)), regardless of whether we compare subsamples sliced by galaxy color or inclination. However, we find statistically larger column densities for blue and face-on galaxies probed along the minor axis (panel (a)).

i.e., a significant chi-squared test corresponds to a significant F-test, and vice versa.

In general, we find that higher velocity material has lower column density values, while higher column density material is only found at lower velocity. This is consistent with previous works (e.g., Churchill et al. 2003). The highest velocity ( $v > |100| \text{ km s}^{-1}$ ), low column density clouds are mostly associated with blue, face-on galaxies probed along the minor axis. There is also a population of  $v \sim |100| \text{ km s}^{-1}$  clouds that are associated with edge-on galaxies probed along the minor axis, though we find a few for major axis galaxies as well. All of these clouds at high velocity are found in absorbers which have higher column density material located near the velocity zero point.

For minor axis galaxies in Figure 5(a), we find that blue galaxies (all inclinations) have significantly larger column densities than red galaxies ( $3.2\sigma$ ) and edge-on galaxies (all colors) have significantly larger column densities than face-on galaxies ( $3.4\sigma$ ). For major axis galaxies in Figure 5(b), we find only a suggestion of larger column densities for edge-on galaxies than face-on galaxies ( $2.9\sigma$ , all colors), though clouds at  $\log N(\text{Mg II}) > 14$  are mainly hosted by edge-on galaxies. Conversely, we find no difference in the column density distribution between blue and red galaxies ( $1.9\sigma$ , all inclinations) along the major axis.

In Figure 6 we compare the cloud column densities and velocities, and the pixel velocities for (a) face-on galaxies and (b) edge-on galaxies, slicing the samples by galaxy color and azimuthal angle. Similar to Figure 5, point colors and the left and bottom histograms represent blue and red galaxy subsamples, while point types and top and right histograms represent

major axis and minor axis subsamples. The indicated significances correspond to the same statistical tests as in Figure 5. Again, the pixel velocity F-test results in Figure 6 follow the TPCF chi-squared test results, with the exception of the test comparing edge-on galaxies probed along the major versus minor axes (panel (b)). In this case the F-test result is significant, where edge-on, major axis galaxies have a slightly larger dispersion in their pixel velocities than for edge-on, minor axis galaxies. Due to the large bootstrap uncertainties on the major axis TPCF, the chi-squared test on the corresponding TPCFs is not significant (see Figure 2(e)).

We find that absorbers around face-on galaxies consist of clouds with column densities that rarely exceed  $\log N(\text{Mg II}) = 14$ . This is in contrast to edge-on galaxies which are more likely to have these higher column density clouds. For face-on galaxies, the column densities of blue and red galaxies are statistically consistent ( $0.3\sigma$ ). Comparing blue galaxies with face-on and edge-on inclinations (for all azimuthal angles), we find that the column densities of the edge-on subsample are larger than those in the face-on subsample ( $4.7\sigma$ , not plotted). We also find that the column densities of the blue, edge-on subsample are larger than the red, edge-on sample ( $4.0\sigma$ ). There are no such differences in the column densities between galaxies probed along the major and minor axes for face-on ( $0.7\sigma$ ), edge-on ( $0.9\sigma$ ), blue ( $1.4\sigma$ , not plotted) or red ( $1.5\sigma$ , not plotted) galaxies.

#### 4. DISCUSSION

The results in the previous section demonstrate that absorber velocity dispersions and cloud column densities of the gas traced by Mg II absorption detected with  $W_r(2796) \geq$

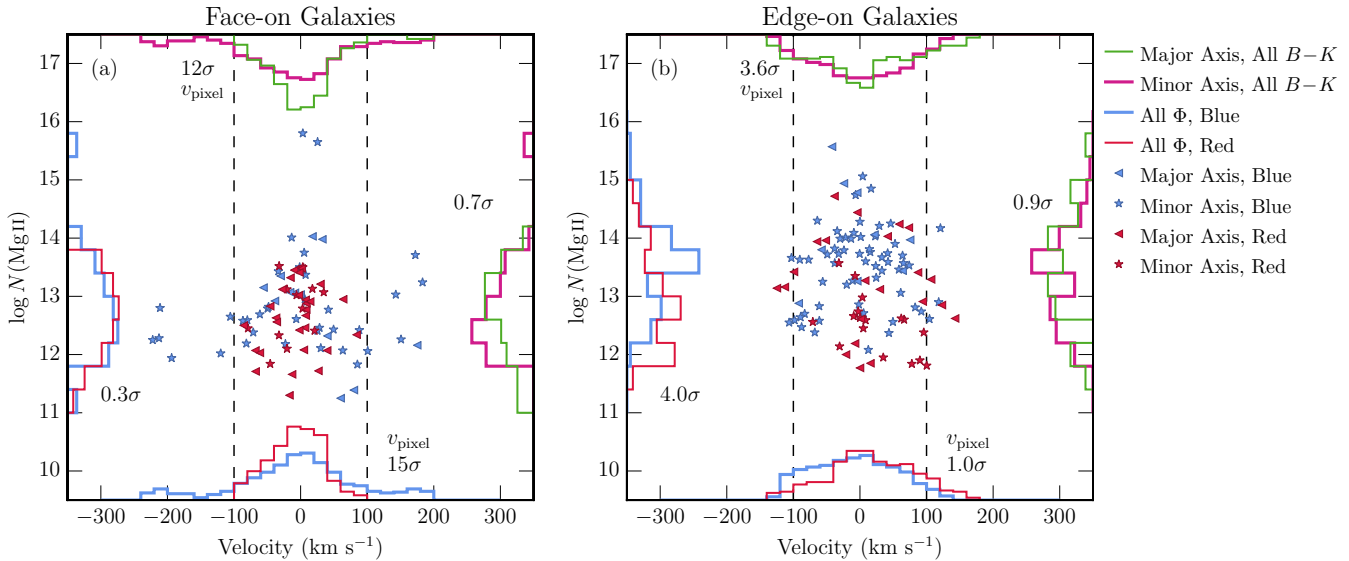


**Figure 6.** Cloud column densities and velocities, and pixel velocities for (a) face-on galaxies ( $i < 57^\circ$ ) and (b) edge-on galaxies ( $i \geq 57^\circ$ ) split by galaxy color and azimuthal angle. Blue galaxies are represented as blue points, red galaxies as red points, galaxies probed along the major axis as triangles, and galaxies probed along the minor axis as stars. Vertical dashed lines are plotted to help guide the reader’s eye between panels. Histograms in each panel represent the distributions of cloud column densities split by (left) galaxy color,  $B-K$ , (right) azimuthal angle,  $\Phi$ , and pixel velocities (rather than cloud velocities) split by (bottom) galaxy color, and (top) azimuthal angle. The quoted significances near the histograms report the results of a KS test between plotted subsamples for the cloud column densities (left and right) and the results of an F-test comparing the variance in the pixel velocity distributions between plotted subsamples for the top and bottom histograms. We find that the cloud column densities for absorbers around face-on galaxies rarely exceed  $\log N(\text{Mg II}) = 14$  (panel (a)), in contrast to edge-on galaxies (panel (b)). For both face-on and edge-on galaxies, we see no difference in the column densities with regard to the azimuthal angle (right histograms). Lastly, we find that the cloud column densities in absorbers around blue galaxies with edge-on inclinations are greater than those for absorbers around blue, face-on galaxies ( $4.7\sigma$ , not plotted) or red, edge-on galaxies ( $4.0\sigma$ , panel (b)).

$0.04 \text{ \AA}$  depend strongly on where the gas is located around isolated galaxies. In particular, we find that absorbers with the largest velocity spreads are associated with blue galaxies that have “face-on” inclinations and are probed along the galaxy projected minor axis. For “edge-on” galaxies, the velocity structure is similar regardless of galaxy color or azimuthal angle. Thus, the absorber velocity spreads (TPCFs) depend mostly on if the galaxy is “star-forming” (using color as a proxy for the star formation rate), or if the galaxy is “face-on.” The cloud column densities depend mostly on galaxy inclination or color, where face-on or red galaxies host absorbers with smaller cloud column densities than those hosted by edge-on or blue galaxies.

Mechanisms in the baryon cycle which could give rise to these differences in velocity structure and column densities of the  $\text{Mg II}$ -absorbing gas include (1) merging satellite galaxies whose gas is either being ejected due to star formation or being stripped by tidal forces, (2) IGM accretion, recycled accretion, and/or rotating material merging onto the galaxy disk, and (3) outflowing gas in star-forming galaxies. In this section, we discuss which mechanisms may most likely contribute to the differences in the observed velocity dispersions and cloud column densities as a function of host galaxy color (as a proxy for star formation) and orientation.

#### 4.1. Merging Satellite Galaxies

Regardless of our results with orientation, previous works have repeatedly shown that the probability of probing a satellite galaxy with quasar absorption lines is low. Martin et al. (2012) found only one satellite galaxy contributing to  $\text{Mg II}$  absorption out of a full sample of over 200 galaxies, corresponding to a probability of finding absorption due to a satellite galaxy of  $< 1\%$ . Tumlinson et al. (2013) used simulations to estimate the cross-section of HI gas bound to satel-

lites and assumed that the internal velocity dispersion of gas in the satellites cannot exceed the maximum circular velocity of the satellite. They found that the mean number of satellites per sightline is well below the number of absorption components per sightline at a given velocity for their sample of HI absorbers. For  $\text{Mg II}$  absorption, Gauthier et al. (2010) examined covering fractions for absorbers around luminous red galaxies (which are comparable to our reddest galaxies) and compared them to the estimated maximum cross-section of satellites in host halos. They found that this maximum cross-section is much lower than the absorber covering fractions at all impact parameters, and therefore satellites are not sufficient for explaining the presence of the majority of absorption around galaxies.

If we assume that the cross-section of satellites is great enough to explain the presence of the majority of  $\text{Mg II}$  absorption, we can investigate the preferential location of satellite galaxies around a larger, central galaxy to determine if satellites could drive our results. Many previous works have examined satellite distributions and the consensus appears to be that, for red galaxies, satellites within the virial radius are preferentially aligned with the central galaxy’s major axis, while there is no preferred alignment for satellites around blue galaxies (with the exception of galaxies in the Local Group; Yang et al. 2006, and references therein). This has been confirmed in recent simulations by Dong et al. (2014). Our color cut defining blue and red galaxies is slightly bluer than that used by Yang et al. (2006) (our  $B-K = 1.399$  cut corresponds to  $g-r = 0.62$ , compared to their cut of  $g-r = 0.83$ ). Our bluer color cut may result in more blue galaxies in our “red” sample than in the Yang et al. (2006) red sample. Since the blue galaxies in Yang et al. have been found to have an isotropic distribution of satellites, we may have a somewhat more isotropic distribution of satellites around red galaxies



for our sample.

We cannot rule out that we may be observing some amount of Mg II absorption due to satellites. However, even though satellites align with the major axis of red galaxies, we find no difference between the TPCFs or column densities of our red galaxy samples along the major and minor axes. The isotropic distribution of satellites around blue galaxies is not consistent with the highly significant differences between the TPCFs of our blue galaxy samples along the major and minor axes. If satellites are the dominant source of Mg II absorption, we would expect the TPCFs to show differences along the major and minor axes in red galaxies (which could be mitigated by our bluer color cut), but show no differences in blue galaxies (which we do find).

We do not have velocity information on the host galaxy–satellite galaxy samples published in Yang et al. (2006). However, the velocity distribution of the satellites around galaxies is unlikely to be the cause of the different absorber kinematic distributions for several reasons. We are measuring the internal velocity dispersions of the absorbers themselves, not the material with respect to the galaxy systemic velocity. We assume our sightlines are unlikely to pass through multiple satellites with a single sightline since the probability of passing through a single galaxy is low ( $< 1\%$ , from above), and probing multiple satellites at once is even lower. Therefore the internal gas velocity distributions of the satellite galaxies would have to show differences for blue central galaxies (to match the TPCFs), but not for red central galaxies. However, if Mg II absorption is due to tidal stripping of or outflows from the satellites, we would expect the satellites around red galaxies (which tend to be located in more massive halos in our sample) to be more disturbed and therefore have larger absorber velocity dispersions than if they were located around blue galaxies, which tend to be less massive in our sample. This is the reverse of our findings.

The galaxies in our sample were drawn from MAGIIICAT (Nielsen et al. 2013b), which contains only galaxies that are isolated to the limits of the data, where no spectroscopically identified neighbor was found within  $D < 100$  kpc or a line-of-sight velocity of  $500 \text{ km s}^{-1}$ . If satellites are present in our sample, they are undetected within both velocity space and impact parameter. Additionally, all of the galaxies were imaged with *HST* and satellite galaxies were not detected in any of the images to the limits of our data. Therefore, if we are probing satellite galaxies, they are below our detection limits (i.e., below roughly  $0.1L_B^*$ , corresponding to a circular velocity of  $\sim 80 \text{ km s}^{-1}$  for these satellites; Nielsen et al. 2013b; Churchill et al. 2013).

#### 4.2. Accretion and Rotation

Previous work examining the low-ionization CGM has found accreting and/or rotating material for edge-on galaxies probed along the projected major axis in the form of absorption that is shifted to one side of the galaxy systemic velocity (e.g., Steidel et al. 2002; Kacprzak et al. 2010; Bouché et al. 2013; Rubin et al. 2012). This is also commonly observed in simulations (e.g., Stewart et al. 2011). Since we do not know whether our absorbers are blueshifted or redshifted with respect to the galaxy as can be determined through the down-the-barrel approach used by Rubin et al. (2012), we cannot say for certain whether our absorbers are accreting or rotating. However, we have examined the properties of this material using absorber velocity dispersions and cloud column

densities for orientations in which accreting and rotating material is expected to be found.

Edge-on galaxies probed along the major axis are most likely to exhibit accreting or rotating material and are the least likely orientation to be contaminated with outflowing material. The line-of-sight velocity for rotation is greatest in edge-on galaxies since the rotation is in the plane of the galaxy. In our sample, this orientation is dominated by absorbers that contain clouds with larger column densities ( $\log N(\text{Mg II}) > 13$ ), most of which have velocities  $v < |100| \text{ km s}^{-1}$ . This is most easily seen as the triangle points in Figure 5(b). We might expect to only see blue galaxies with absorption in this orientation due to the red galaxies having their star formation quenched from a lack of a gas reservoir, but the subsample is populated by both blue and red galaxies.

We could be seeing recycled accretion in galaxies of all colors from past outflows (e.g., Oppenheimer et al. 2010). However, accretion onto galaxies provides fuel for star formation, which we do not infer for our red galaxies. It is possible that this material is rotating around the galaxy and not accreting onto the galaxy, especially for the red galaxies, though we cannot tell if this is the case for the data presented here as our velocities are not shifted with respect to the galaxy systemic velocity. Some mechanism may be suppressing star formation in the red galaxies, but this mechanism is not present in blue galaxies. It is also possible that some of the red galaxies we have observed are in fact dusty, star-forming galaxies that are currently accreting material, especially since our  $B-K$  color cut does include Sbc SED types in with the “red” galaxy subsample (for details concerning our  $B-K$  color calculations, see Nielsen et al. 2013b). This is less likely because we would have observed signatures of outflows in both blue and red galaxies, unless dusty, star-forming galaxies are rare in our sample. We do not yet have the information needed to calculate the star formation rates to determine if we have dusty, star-forming galaxies in our sample.

It is interesting that we find no significant difference in the TPCFs of blue and red galaxies probed along the major axis (for all  $i$ ) or in edge-on inclinations (for all  $\Phi$ ) in Figures 3(a) and 4(b), respectively. This suggests that the velocity structure of absorbers along the major axis or for edge-on galaxies does not depend on the star formation rate of the host galaxy, and likely depends only on mass. This fits in with the accretion or rotating gas picture, which, unlike outflows, should not depend on the star formation rate unless the star formation rate is so great as to prevent accretion and/or remove the gas reservoir. Also interesting is that, for all  $B-K$ , the absorber velocity dispersions depend on inclination for the major axis sample in Figure 2(c). Along the major axis, the absorber velocity dispersion is greater for edge-on galaxies than for face-on galaxies, and this may be due to rotating gas whose line-of-sight velocity is maximized in edge-on inclinations, while the vertical velocity dispersions in the disks of galaxies is small. The column densities may also be greater for edge-on galaxies than for face-on galaxies along the major axis (Figure 5(b)). This could indicate that the accreting or rotating material for the edge-on galaxies is more coherent, i.e., the path lengths or amount of material are larger than for face-on galaxies.

#### 4.3. Outflows

Absorption line studies have frequently found evidence for outflows as blueshifted absorption in face-on galaxies (e.g., Rubin et al. 2014) or as enhanced equivalent widths along the projected minor axis for edge-on galaxies (e.g., Bordoloi et al.

2011; Kacprzak et al. 2012). Therefore we also can associate the kinematics results for our blue, face-on and minor axis subsamples with outflows. Again, we cannot say for certain if our absorbers are actually entrained in outflowing material so we instead focus on possible absorption properties of the absorbers for orientations in which outflows are most likely to occur.

For blue, edge-on galaxies probed along the minor axis (blue triangles in Figure 5(a)), we found a group of lower column density ( $\log N(\text{Mg II}) < 13$ ), higher velocity ( $v \sim |100| \text{ km s}^{-1}$ ) material. This is similar to Fox et al. (2015) who used a background quasar whose line of sight passes through the biconical Fermi Bubbles at the Milky Way Galactic center, where the Milky Way in this case is similar to our edge-on, minor axis subsample. They reported a complex absorption profile with two high-velocity metal absorption components at  $v_{\text{LSR}} \sim \pm 250 \text{ km s}^{-1}$  with  $\log N(\text{Si II}) \sim 13.2$ . They associate these components with cool gas that has been entrained in the near and far sides of an outflow from the galactic center. In our sample, comparable components have similar column densities, but a lower velocity with respect to the bulk of the absorption, which may be due to the fact that we are probing outflows at much larger impact parameters than Fox et al. (2015);  $D > 20 \text{ kpc}$  compared to  $D = 2.3 \text{ kpc}$ . This suggests that the low column density clouds we find in our edge-on, minor axis galaxies may also be associated with fragmented cool gas entrained in outflows.

In our subsample consisting of blue, face-on galaxies probed along the minor axis (blue circles in Figure 5(a)), the absorbers are dominated by low column density material ( $\log N(\text{Mg II}) < 14$ , where most of the clouds are  $\log N(\text{Mg II}) \leq 13$ ), with high velocity components at  $v > |100| \text{ km s}^{-1}$ . This material is also similar to the absorber found by Fox et al. (2015). We suggest that the velocities are larger for our face-on galaxies than for our edge-on galaxies along the minor axis because we are observing down into the outflow (i.e., close to the down-the-barrel approach) as opposed to across the outflow. We expect the line-of-sight velocity dispersions to be larger for the face-on sample as the biconical outflows are pointed toward (or away from) the observer, and this is observed in our face-on, blue galaxy subsample TPCFs.

The larger column density ( $\log N(\text{Mg II}) > 13$ ), lower velocity ( $v \lesssim |50| \text{ km s}^{-1}$ ) clouds for blue, edge-on galaxies probed along the minor axis (seen in Figure 5(a) as blue triangles), suggest that we are observing more material, a larger path length, a larger metallicity, or ionization conditions that are more conducive to Mg II absorption than for the face-on, minor axis galaxies (blue circles) described in the previous paragraph. Since the material probed in both of these orientations is most likely outflows, we do not expect the metallicity or the ionization conditions to differ for these two subsamples, and therefore should not be the cause of the enhanced column densities for the edge-on sample compared to the face-on sample. However, Veilleux et al. (2005) listed large variations in the metallicity and ionization levels between clouds as a possible signature of outflows in quasar absorption lines. If this were the case here, we should also see the large column density clouds ( $\log N(\text{Mg II}) > 13$ ) for face-on galaxies, but they are nonexistent in our sample. Differences in the column densities with inclination therefore hint at probing larger amounts of gas or larger path lengths for the lowest velocity clouds associated with outflows in edge-on galaxies (compared to face-

on galaxies), an effect that may be due to the geometry of the gas flow.

In contrast to the blue galaxies, we find very small absorber velocity dispersions for red galaxies in face-on, minor axis orientations (red circles in Figure 5(a)). We suggest that this is due to a lack of current outflows. This is supported by the fact that redder galaxies typically have lower star formation rates and do not typically drive outflows. We caution that this subsample is small, which may indicate that outflows in red galaxies for this orientation are rare rather than nonexistent in general.

## 5. SUMMARY AND CONCLUSIONS

We examined the dependence of gas kinematics and cloud column densities on galaxy rest-frame  $B-K$  color, azimuthal angle, and inclination for a subset of 30 isolated MAGIIICAT (Nielsen et al. 2013b) galaxies. Each galaxy was imaged with *HST* and was modeled with GIM2D to obtain galaxy orientations. In each case, we have a high-resolution optical spectrum of an association background quasar within  $20 < D < 110 \text{ kpc}$  for detailed kinematic analysis. To characterize the absorber gas kinematics, we examined only those absorbers detected with  $W_r(2796) \geq 0.04 \text{ \AA}$  and calculated pixel-velocity two-point correlation functions (TPCFs) for galaxy color, azimuthal angle, and inclination subsamples.

Our findings include the following:

1. Absorption TPCFs with the longest high velocity separation tails (the largest velocity dispersions) are associated with blue galaxies, face-on galaxies, and galaxies probed along the minor axis. Conversely, the narrowest TPCF is associated with red, face-on galaxies. The velocity structure in the absorbers hosted by edge-on galaxies is similar regardless of galaxy color or azimuthal angle, and we find a lack of differences for red galaxies with azimuthal angle as well as for blue and red galaxies probed along the projected major axis.
2. Examining cloud column densities and velocities, we find, in general, that the highest velocity clouds with respect to the optical depth weighted mean of absorption ( $z_{\text{abs}}$ ) have small column densities, while the largest column density clouds are located at small velocities. When slicing our sample by galaxy color and inclination, we find that the column densities are larger for edge-on galaxies and blue galaxies than for face-on galaxies and red galaxies, respectively. The column densities show no dependence on azimuthal angle, however.
3. We find large absorber velocity dispersions and large column density clouds at low velocity for edge-on galaxies probed along the major axis, an orientation that is associated with gas accreting onto and/or rotating around galaxies. The velocity structure of the absorbers for this orientation does not depend on galaxy color and, by proxy, star formation rate. The large absorber velocity dispersions for this orientation may be due to rotating gas whose line-of-sight velocity is maximized due to the edge-on inclination, especially compared to the smaller velocity dispersions for face-on galaxies along the major axis. The large column density clouds may indicate that accreting and/or rotating material is fairly coherent, where the path lengths or amount of gas probed is larger than for other subsamples.

4. We associate the largest absorber velocity dispersions and smaller column density clouds at higher velocity for blue, face-on galaxies probed along the minor axis and for blue, edge-on galaxies along the minor axis with bipolar outflows, which are commonly observed in these orientations. The behavior of this material and the fact that it is located in regions which are associated with outflows may be an indication that the material probed by Mg II absorption is fragmented material entrained in outflows. These absorbers are similar to the absorption associated with the Fermi Bubbles in the Milky Way Galaxy (Fox et al. 2015). Larger column density clouds at low velocity are present for the blue, edge-on galaxies probed along the minor axis, and since comparable components are lacking for the face-on sample, we suggest that the path lengths of these structures are larger, possibly a geometry effect. For the smallest column density clouds ( $\log N(\text{Mg II}) \lesssim 13$ ), the cloud velocities (and absorber velocity dispersions) are greater for the face-on galaxies than edge-on galaxies. We attribute this to looking down into the outflow for face-on galaxies, and across the outflow for edge-on galaxies. Conversely, the very small absorber velocity dispersions for red galaxies at these orientations suggests that outflows are not active, a result of star formation having possibly been quenched.
5. Merging satellite galaxies may contribute to the observed Mg II absorption but are not expected to dominate the absorption due to their cross-section being too low. If they did dominate, then we would expect differences in the TPCFs to correspond to the preferred locations of the satellites around galaxies (isotropic distribution for blue galaxies and along the major axis for red galaxies), but this is not the case. We also do not expect the velocities of the satellites to have much of an effect on our TPCFs because it is unlikely that our sightlines are hitting multiple satellites at once, as the probability of detecting a single satellite is  $\lesssim 1\%$  (Martin et al. 2012). Since red galaxies tend to be more massive than blue, we would expect larger internal gas velocity dispersions for satellites hosted by red central galaxies due to tidal stripping or outflows from the satellites themselves, but we do not find this to be the case.

This work shows that the velocity structure and cloud column densities of Mg II absorbers depend on a combination of galaxy orientations and colors (and likely other galaxy properties not included in this work), not just one or two properties at a time as has been commonly examined in the past. For example, when observing edge-on galaxies, absorption could be probing accretion along the major axis, or outflows along the minor axis. In this case, the outflows will dominate the absorption signature and the information for accretion will likely be lost, which may contribute to the low covering fractions found for accreting material.

We also find that while the equivalent width of an absorption profile provides a useful diagnostic for generally determining what type of material is being studied, considering both the velocity structure (in terms of the velocity spread or dispersion) and cloud column densities of absorbers with galaxy orientation is important for probing the details of gas flows. This is evident in the fact that absorbers probing outflows in face-on galaxies may have large equivalent widths because of the large velocity spread in the absorbers,

whereas outflows in edge-on, minor axis galaxies may have large equivalent widths mainly due to large column density clouds. Modeling the ionization conditions and metallicities in the clouds would also be beneficial, as large cloud-cloud variations in outflows have been suggested by Veilleux et al. (2005), but this is beyond the scope of the present work.

Future work might include examining mock quasar absorption line spectra in simulations for a variety of galaxy colors (or star formation rate and mass) and orientations to better understand the origin of the absorber velocity structure and cloud column densities. By applying our analysis to simulations, we not only obtain a more physical explanation for what we observe, but we also help constrain the CGM in simulations. Observationally, a larger sample of galaxies with *HST* images and high-resolution spectra would allow us to slice the sample by galaxy color, azimuthal angle, and inclination to better explore the multivariate dependence of absorber properties on the host galaxy and its baryon cycle. Our current sample is only large enough to slice by two galaxy properties in the TPCFs, though we have presented all three properties in Figures 5 and 6.

It would also be useful to obtain estimates of the absorber metallicities to further understand whether we are probing cold-mode accretion, recycled accretion, satellite material, and/or outflows. Metallicities are important to help distinguish between accretion and outflows, where accreting material is expected to have lower metallicities than outflowing material (see Lehner et al. 2013, and references therein). Comparable metallicities across all galaxy orientations might indicate that Mg II absorption is primarily associated with outflows and recycled accretion, not cold-mode accretion. Lastly, determining the star formation rates of the galaxies in our sample is important to identify any possible dusty, star-forming galaxies which may be contaminating the results of our red galaxy samples. The galaxy star formation rates provide a more physical indicator of ongoing star formation than galaxy color.

We thank C. Steidel for providing a reduced HIRES/Keck quasar spectrum. This material is based upon work supported by the National Science Foundation under Grant No. 1210200 (NSF East Asia and Pacific Summer Institutes). N.M.N. was also partially supported through a NMSGC Graduate Fellowship and a Graduate Research Enhancement Grant (GREG) sponsored by the Office of the Vice President for Research at New Mexico State University. G.G.K. acknowledges the support of the Australian Research Council through the award of a Future Fellowship (FT140100933). M.T.M. thanks the Australian Research Council for Discovery Project grant DP130100568 which supported this work.

## REFERENCES

- Barton, E. J., & Cooke, J. 2009, *AJ*, 138, 1817  
 Bergeron, J., & Boissé, P. 1991, *A&A*, 243, 344  
 Bergeron, J., & Stasińska, G. 1986, *A&A*, 169, 1  
 Bordoloi, R., Lilly, S. J., Kacprzak, G. G., & Churchill, C. W. 2014a, *ApJ*, 784, 108  
 Bordoloi, R., Lilly, S. J., Knobel, C., et al. 2011, *ApJ*, 743, 10  
 Bordoloi, R., Lilly, S. J., Hardmeier, E., et al. 2014b, *ApJ*, 794, 130  
 Bouché, N., Hohensee, W., Vargas, R., et al. 2012, *MNRAS*, 426, 801  
 Bouché, N., Murphy, M. T., Kacprzak, G. G., et al. 2013, *Science*, 341, 50  
 Churchill, C. W. 1997, PhD thesis, University of California, Santa Cruz  
 Churchill, C. W., Kacprzak, G. G., & Steidel, C. C. 2005, in *IAU Colloq. 199: Probing Galaxies through Quasar Absorption Lines*, ed. P. Williams, C.-G. Shu, & B. Menard, 24–41  
 Churchill, C. W., Mellon, R. R., Charlton, J. C., et al. 2000, *ApJS*, 130, 91

- Churchill, C. W., Trujillo-Gomez, S., Nielsen, N. M., & Kacprzak, G. G. 2013, *ApJ*, 779, 87
- Churchill, C. W., & Vogt, S. S. 2001, *AJ*, 122, 679
- Churchill, C. W., Vogt, S. S., & Charlton, J. C. 2003, *AJ*, 125, 98
- Danovich, M., Dekel, A., Hahn, O., Ceverino, D., & Primack, J. 2015, *MNRAS*, 449, 2087
- Danovich, M., Dekel, A., Hahn, O., & Teyssier, R. 2012, *MNRAS*, 422, 1732
- Dong, X. C., Lin, W. P., Kang, X., et al. 2014, *ApJ*, 791, L33
- Evans, J. L. 2011, PhD thesis, New Mexico State University
- Ford, A. B., Davé, R., Oppenheimer, B. D., et al. 2014, *MNRAS*, 444, 1260
- Fox, A. J., Bordoloi, R., Savage, B. D., et al. 2015, *ApJ*, 799, L7
- Gauthier, J.-R., Chen, H.-W., & Tinker, J. L. 2010, *ApJ*, 716, 1263
- Guillemin, P., & Bergeron, J. 1997, *A&A*, 328, 499
- Kacprzak, G. G., Churchill, C. W., Ceverino, D., et al. 2010, *ApJ*, 711, 533
- Kacprzak, G. G., Churchill, C. W., Evans, J. L., Murphy, M. T., & Steidel, C. C. 2011, *MNRAS*, 416, 3118
- Kacprzak, G. G., Churchill, C. W., & Nielsen, N. M. 2012, *ApJ*, 760, L7
- Kacprzak, G. G., Churchill, C. W., Steidel, C. C., & Murphy, M. T. 2008, *AJ*, 135, 922
- Kacprzak, G. G., Cooke, J., Churchill, C. W., Ryan-Weber, E. V., & Nielsen, N. M. 2013, *ApJ*, 777, L11
- Kacprzak, G. G., Martin, C. L., Bouché, N., et al. 2014, *ApJ*, 792, L12
- Lan, T.-W., Ménard, B., & Zhu, G. 2014, *ApJ*, 795, 31
- Law, D. R., Steidel, C. C., Erb, D. K., et al. 2009, *ApJ*, 697, 2057
- Lehner, N., Howk, J. C., Tripp, T. M., et al. 2013, *ApJ*, 770, 138
- Martin, C. L., Shapley, A. E., Coil, A. L., et al. 2012, *ApJ*, 760, 127
- Nielsen, N. M., Churchill, C. W., & Kacprzak, G. G. 2013a, *ApJ*, 776, 115
- Nielsen, N. M., Churchill, C. W., Kacprzak, G. G., & Murphy, M. T. 2013b, *ApJ*, 776, 114
- Nielsen, N. M., Churchill, C. W., Kacprzak, G. G., Murphy, M. T., & Evans, J. L. 2015, *ApJ*, submitted
- Oppenheimer, B. D., Davé, R., Kereš, D., et al. 2010, *MNRAS*, 406, 2325
- Rao, S. M., & Turnshek, D. A. 2000, *ApJS*, 130, 1
- Rigby, J. R., Charlton, J. C., & Churchill, C. W. 2002, *ApJ*, 565, 743
- Rubin, K. H. R., Prochaska, J. X., Koo, D. C., & Phillips, A. C. 2012, *ApJ*, 747, L26
- Rubin, K. H. R., Prochaska, J. X., Koo, D. C., et al. 2014, *ApJ*, 794, 156
- Rubin, K. H. R., Weiner, B. J., Koo, D. C., et al. 2010, *ApJ*, 719, 1503
- Rudie, G. C., Steidel, C. C., Trainor, R. F., et al. 2012, *ApJ*, 750, 67
- Simard, L., Willmer, C. N. A., Vogt, N. P., et al. 2002, *ApJS*, 142, 1
- Steidel, C. C., Dickinson, M., Meyer, D. M., Adelberger, K. L., & Sembach, K. R. 1997, *ApJ*, 480, 568
- Steidel, C. C., Dickinson, M., & Persson, S. E. 1994, *ApJ*, 437, L75
- Steidel, C. C., Erb, D. K., Shapley, A. E., et al. 2010, *ApJ*, 717, 289
- Steidel, C. C., Kollmeier, J. A., Shapley, A. E., et al. 2002, *ApJ*, 570, 526
- Steidel, C. C., & Sargent, W. L. W. 1992, *ApJS*, 80, 1
- Stewart, K. R., Kaufmann, T., Bullock, J. S., et al. 2011, *ApJ*, 738, 39
- Tumlinson, J., Thom, C., Werk, J. K., et al. 2011, *Science*, 334, 948
- . 2013, *ApJ*, 777, 59
- Veilleux, S., Cecil, G., & Bland-Hawthorn, J. 2005, *ARA&A*, 43, 769
- Weiner, B. J., Coil, A. L., Prochaska, J. X., et al. 2009, *ApJ*, 692, 187
- Werk, J. K., Prochaska, J. X., Thom, C., et al. 2013, *ApJS*, 204, 17
- Yang, X., van den Bosch, F. C., Mo, H. J., et al. 2006, *MNRAS*, 369, 1293